Recent Advances in Rh/CGO Co-Impregnated $La_{0.20}Sr_{0.25}Ca_{0.45}TiO_3$ Anodes for Solid Oxide Fuel Cells: Evaluation of Upscaling and Durability

R. Price [a], U. Weissen [b], M. C. Verbraeken [a] J. G. Grolig [b], A. Mai [b] and J. T. S. Irvine [a]

[a] School of Chemistry, University of St Andrews, St Andrews, Fife, KY16 9ST, UK
[b] HEXIS AG, Zum Park 5, CH-8404 Winterthur, Switzerland

Recent research carried out at the University of St Andrews and HEXIS has focussed on a novel A-site deficient perovskite: $La_{0.20}Sr_{0.25}Ca_{0.45}TiO_3$ ($LSCT_{A-}$) as a potential replacement material for the Ni-based cermet. $LSCT_{A-}$ is a mixed ionic and electronic conductor, which exhibits a high effective electrical conductivity for this class of limited conductivity perovskite, allowing a single-phase anode 'backbone' to be employed and removing the challenges associated with utilisation of a structural Ni phase. Co-impregnating this 'backbone' with a variety of transition/platinum group metals, as well as $Ce_{0.80}Gd_{0.20}O_{1.90}$ (CG20), produces intricately nanostructured anode materials with high electrocatalytic activity for fuel oxidation. Here we provide an overview of the first 'all-oxide' SOFC stack test at HEXIS, as well as an in depth exploration of the 'powder-to-power' development of these co-impregnated $LSCT_{A-}$ anodes including: ceramic processing, catalyst selection, short-term testing, characterisation by AC impedance spectroscopy and durability testing of promising candidate catalyst systems.

Introduction

Solid Oxide Fuel Cells (SOFC) have typically employed the Ni-based cermet anode material, in both academic and commercial research, to date. However, redox instability, Ni-particle agglomeration, as well as coking intolerance and sulphur poisoning (1), in unprocessed natural gas streams, are challenges that need to be overcome in next generation anode materials.

$La_{0.20}Sr_{0.25}Ca_{0.45}TiO_3$ ($LSCT_{A-}$) is a A-site deficient perovskite which exhibits high effective electrical conductivity (2) and ionic conductivity (3,4), in addition to redox stability (5). This, therefore, makes $LSCT_{A-}$ a promising candidate for a single-phase anode 'backbone' microstructure which does not degrade as a result of agglomeration of the metallic Ni-phase contained in the state-of-the-art Ni-based cermet materials. When impregnated with ceria-based coatings and particles of transition or platinum group metals, the $LSCT_{A-}$-based anode microstructures give rise to excellent performance during SOFC testing (2, 4 – 6).

Following on from initial collaborative work on Ni/CeO_2 and Ni/CG20 co-impregnated $LSCT_{A-}$ anodes (5,6), recent research sought to improve the durability of these SOFC with the ultimate aim of upscaling this technology to an industrially relevant scale at HEXIS AG.

In this paper we provide an overview of the development of co-impregnated $LSCT_{A-}$ anodes, focussing on the Rh/CG20 impregnated catalyst system. A brief description of the first-generation work, carried out by Verbraeken *et al.*, including the first reported 'all-oxide' SOFC stack test using co-impregnated $LSCT_{A-}$ anodes will be provided. Subsequently, a more detailed discussion of the second-generation research will be given, covering the optimisation of the $LSCT_{A-}$ anode 'backbone' and evaluation of candidate catalyst systems, indicating that Area Specific Resistances (ASR) of as low as 0.39 Ω cm^2, at 900 °C, can be achieved using nanoparticles of platinum group metals, as opposed to the traditional Ni nanoparticular catalyst (4). In addition, an AC impedance spectroscopic study of the rate limiting processes associated with the operation of SOFC will be presented, including the assignment of limiting processes to specific components within the SOFC. Finally, details on the durability of SOFC containing a Rh/CG20 co-impregnated $LSCT_{A-}$ anode will be provided.

Previous Research

In 2012, Verbraeken *et al.* presented work relating to SOFC containing Ni/CG20 and Ni/CeO_2 co-impregnated $LSCT_{A-}$ anodes, evaluating their suitability as replacements for the Ni-based cermet standard anode material. In first-generation button cell tests, the aforementioned SOFC showed excellent redox stability and ASR which were comparable to those achieved using state-of-the-art anodes at HEXIS (Figure 1 (5)).

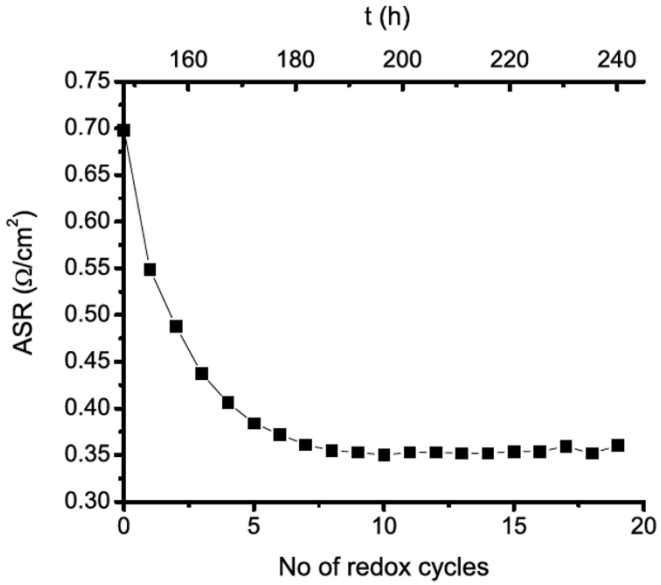

Figure 1. Evolution of ASR as a function of redox cycling and time for a SOFC containing a $LSCT_{A-}$ anode co-impregnated with 5 wt. % Ni and 10 wt. % CeO_2, reported by Verbraeken *et al.* (5).

However, it was highlighted that due to the limited electronic conductivity of these $SrTiO_3$-based anode 'backbone' materials, poor lateral electronic conductivity may arise if the anode layers were made to thin, *i.e.* preventing the electrons generated at the Triple Phase Boundary (TPB) from reaching the current collector or Metallic Interconnect (MIC) plates in a SOFC stack and increasing the ohmic resistance of the SOFC. Due to the

promising initial performance of this novel anode catalyst system, it was implemented into a full 60-cell SOFC stack within the HEXIS Galileo 1000 N micro-Combined Heat and Power (μ-CHP) unit (6). Of the nominal 1 kW power output of this unit, an impressive 700 W was attained at the first attempt of upscaling. However, over the course of ~600 hours, the power output dropped to ~250 W and the stack performance had degraded substantially. Post-mortem Scanning Electron Microscopy (SEM) revealed that thin and dense (*i.e.* non-optimal) anode microstructures had given rise to poor current distribution, the creation of localised temperature 'hotspots' and, therefore, severe agglomeration of the Ni nanoparticles up to 400 nm (6). Therefore, it was concluded that optimisation of the $LSCT_{A-}$ anode 'backbone' microstructure was required to prevent this from occurring in future stack tests. Thus, this optimisation became the initial focus of the second-generation research that we present here.

Experimental

Preparation of SOFC

SOFC were prepared by screen printing anode and cathode inks onto pre-sintered, 160 μm thick, 6 molar % scandia-stabilised-zirconia (6ScSZ) electrolytes (supplied by HEXIS) before being sintered in air. The anode 'backbone' material, $La_{0.20}Sr_{0.25}Ca_{0.45}TiO_3$, supplied by Treibacher Industrie AG was sintered up to 1350 °C for 2 hours in air, whilst $LSCT_{A-}$ powder supplied by Praxair Specialty Ceramics was fired up to 1100 °C for 2 hours in air. State-of-the-art LSM-8YSZ/LSM (LSM = $La_{0.76}Sr_{0.19}MnO_3$ (Praxair Specialty Ceramics) and 8YSZ = 8 mol. % yttria-stabilised-zirconia (Daiichi Kigenso Kagaku Kogyo Co. Ltd.)) double layer cathodes were sintered up to 1100 °C for 2 hours in air. Details of screen printing ink formulations are reported elsewhere (2,4).

SOFC employed for the 'component variation' testing were prepared in a similar manner to that which is outlined above, however the composition and microstructural properties of the anode, cathode and electrolyte were altered in order to assign processes found in the AC impedance spectra of these SOFC to specific components.

Alternative Cathodes. Another LSM-YSZ/LSM cathode was produced using a LSM powder with a smaller particle size than the 'standard' LSM powder (d_{50} = 1.1 μm vs. 1.4 μm, respectively). This cathode was also sintered up to 1100 °C for 2 hours in air. In addition, a CGO/LSCF-CGO/LSCF (LSCF = $La_{0.60}Sr_{0.40}Co_{0.20}Fe_{0.80}O_{3+\delta}$ (Praxair Specialty Ceramics) and CGO = $Ce_{0.90}Gd_{0.10}O_{1.95}$ (HEXIS)) triple layer cathode was screen printed and sintered in air. The CGO barrier layer was sintered up to 1225 °C for 2 hours, whilst the LSCF-CGO (50:50 wt. %) and pure LSCF components were sintered up to 1050 °C for 2 hours.

Alternative Anodes. In order to characterise the AC impedance response of the anode, a single-phase LSCM anode (LSCM = $La_{0.73}Sr_{0.24}Cr_{0.50}Mn_{0.50}O_{3+\delta}$ (Praxair Specialty Ceramics)) and a state-of-the-art Ni-YSZ (40:60 wt. %) anode (Ni supplied by Novamet) were both screen printed and sintered up to 1350 °C for 2 hours in air.

Alternative Electrolytes. Finally, a SOFC with a 8YSZ electrolyte (HEXIS) was produced in order to identify contributions, other than the ohmic resistance, that pertain to electrolyte processes.

Addition of electrocatalytically active phases to the $LSCT_{A-}$ anode 'backbone' was achieved through the process of wet impregnation. Firstly, a 0.5 M solution of the nitrate precursors of $Ce_{0.80}Gd_{0.20}O_{1.90}$ (CG20) was produced by dissolving the required molar ratios of $Ce(NO_3)_3.6H_2O$ and $Gd(NO_3)_3.6H_2O$ (99 %, Sigma-Aldrich) in ethanol. A droplet of the solution was added to the surface of the $LSCT_{A-}$ anode 'backbone' before being dried at 80 °C and then calcined up to 500 °C for 30 minutes, to yield the CG20 component. The same process was then used impregnate the Ni, Pd, Pt, Rh and Ru metal oxide phases into the anode 'backbone' and details of the precursor solutions are presented in previous work (4).

Testing and Characterisation of SOFC

Short-term SOFC testing at St Andrews was carried out in a 'sealless' setup which allowed the formation of a post-cell combustion zone, in accordance with the HEXIS concept and to provide comparable data to those collected in the test setups at HEXIS (4). Alumina felt gas diffusion gaskets were used to insulate the SOFC from the electrically conductive cell housing and contacting of the electrodes was achieved using Au mesh, wires and paste. SOFC were tested using a fuel gas of 3 % H_2O/97 % H_2 and an oxidant gas of compressed air (both at flow rates of 250 mL min^{-1}), up to 900 °C (4). AC impedance spectra were collected at 0.8 V with an excitation amplitude of 50 mV, using a Solartron SI 1280B Electrochemical Measurement System.

Short-term and durability testing of SOFC carried out at HEXIS used similar test setups to those previously described. In this case, Au mesh (without paste) was used to contact the cathode whilst, Ni paste and mesh were used to contact the anode. The fuel gas employed was non-humidified H_2 (1 % H_2O/99 % H_2) at a flow rate of 200 mL min^{-1} and the oxidant gas used was compressed air at a flow rate of 420 mL min^{-1}. AC impedance spectra were collected at 300 mA cm^{-2} with an excitation amplitude of 10 mA, using a Zahner Elektrik IM6ex impedance spectrometer.

Scanning Electron Microscopy (SEM) of the $LSCT_{A-}$ anode 'backbone' microstructures was carried out using a JEOL JSM 6700F FEG-SEM.

Results and Discussion

Optimisation of the $LSCT_{A-}$ Anode Microstructure and Short-Term SOFC Testing

In order to prevent the previously mentioned issues with lateral electronic conductivity and poor current distribution, the $LSCT_{A-}$anode 'backbone' microstructure as optimised using thick-film ceramic processing techniques. Information on the detailed ceramic processing of this material are reported elsewhere (2,7), however, it was found that screen printing of anode layers using a 75 wt. % $LSCT_{A-}$ loading ink and a 230 mesh count (per inch) screen yielded well-connected 'backbone' microstructures with sufficient porosity to allow impregnation of electrocatalysts and facile gas diffusion during testing (Figure 2)

(2,4). Four-point DC conductivity testing of this anode microstructure (printed on a 8YSZ electrolyte) in a half-cell format indicated that an effective conductivity of 21 S cm^{-1} could be achieved at 900 °C or 17 S cm^{-1} at 850 °C (2). This was thought to be sufficient to prevent severe ohmic losses within the $LSCT_{A-}$ anode 'backbone'.

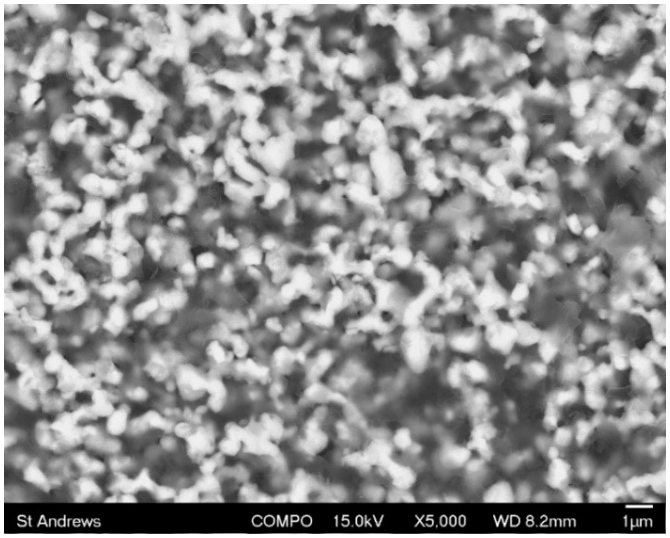

Figure 2. SEM image of the $LSCT_{A-}$ 'backbone' microstructure that resulted from screen printing of a 75 wt. % solids loading ink with a 230 mesh count (per inch) screen and sintering at 1350 °C for 2 hours in air.

Subsequently, this microstructure was employed as the anode 'backbone' in full SOFC, but due to the low electrocatalytic activity of this material, additional electrocatalysts were introduced using the process of catalyst co-impregnation. Here, CG20 was first added to anode microstructure, to further improve ionic and electronic conductivity, in addition to promoting reduced mobility of the metallic catalyst phase, before the metallic component was introduced to increase the TPB length available for H_2 oxidation. Five co-impregnated $LSCT_{A-}$ anode catalyst systems (Ni/CG20, Pd/CG20, Pt/CG20, Rh/CG20 and Ru/CG20) were evaluated during short-term SOFC testing, using 3% H_2O/97 % H_2 as a fuel gas and compressed air as an oxidant gas. The complex plane AC impedance spectrum for each anode catalyst system, collected at 0.8 V and 900 °C, is presented in Figure 3. As previously described (4), these spectra typically exhibit 3 rate limiting processes: i) a high frequency anode charge transfer arc (2,4,5), ii) a mid-frequency cathode related process (4,8) and iii) a low-frequency gas conversion arc (4,5,9). Despite the SOFC containing the Pd/CG20 co-impregnated $LSCT_{A-}$ anode showing the lowest ASR (0.39 Ω cm^2), the Rh/CG20 co-impregnated $LSCT_{A-}$ anode showed the absence of a high-frequency anode charge transfer arc, making this system particularly interesting for further development.

Assignment of Rate Limiting Processes using AC Impedance Spectroscopy

In order to further clarify the components to which rate limiting processes belong, SOFC were subjected to AC impedance spectroscopic analysis, during testing at HEXIS, as a function of temperature and current. Figures 4 and 5 show the complex plane AC impedance spectra for a SOFC containing a Rh/CG20 co-impregnated $LSCT_{A-}$ anode, a 6ScSZ electrolyte and a LSM-YSZ/LSM cathode as a function of temperature and current, respectively. The three processes, previously mentioned, may be easily identified within these spectra, in addition to another high-frequency process (f_{max} = 16,000 Hz) which

appears to elongate the lower-frequency anode charge transfer arc (f_{max} = 6,500 Hz). The higher-frequency process shows slight activation with increasing temperature and current density and, therefore, most likely relates to a charge transfer process. As a cathode response is not expected in this frequency domain (4), it is tentatively assigned as an anode charge transfer process. As expected, both the lower-frequency anode charge transfer process and the cathode charge transfer process are thermally activated, whilst the gas conversion process shows no temperature dependence. These assignments are further confirmed by the current sweep data which show that the anode charge transfer and gas conversion processes reduce in polarisation resistance with increasing current (and $p(H_2O)$). The cathode charge transfer process is strongly affected by the magnitude and frequency domain of the adjacent processes, however, current density does not affect it significantly.

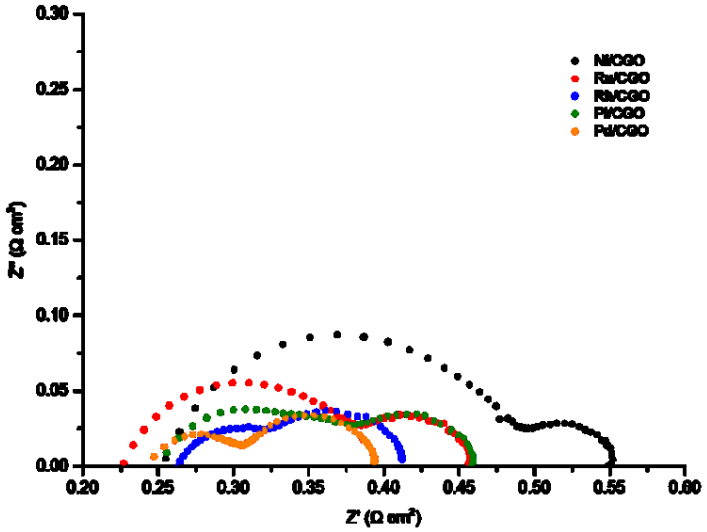

Figure 3. Comparative complex plane AC impedance spectra of SOFC containing a variety of metal/CG20 co-impregnated $LSCT_{A-}$ anodes, collected using the St Andrews test setup, at 0.8 V and 900 °C.

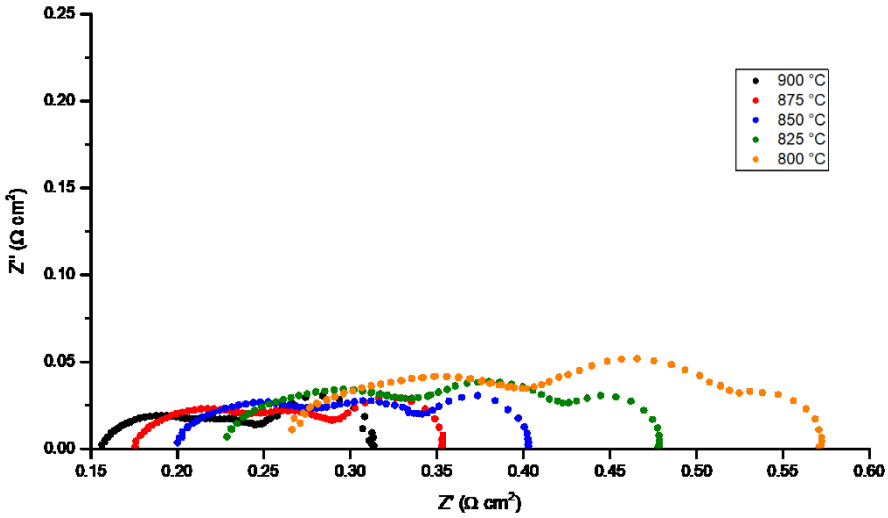

Figure 4. Complex plane AC impedance spectra for a SOFC containing a Rh/CG20 co-impregnated $LSCT_{A-}$ anode, collected at 300 mA cm^{-2} as a function of temperature using the HEXIS test setups.

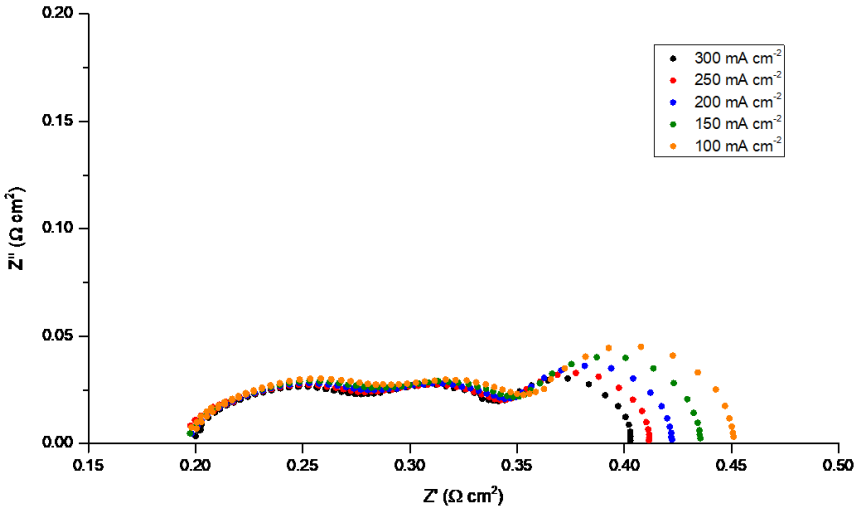

Figure 5. Complex plane AC impedance spectra for a SOFC containing a Rh/CG20 co-impregnated $LSCT_{A-}$ anode, collected at 850 °C as a function of current density using the HEXIS test setups.

Another way to unequivocally confirm the assignment of processes is to simply vary the individual components of the SOFC and measure the resultant AC impedance response. Table I summarises the components used in each SOFC produced for component variation testing. Figure 6 shows the Bode format AC impedance spectra collected for SOFC with different cathodes. Manufacturing a LSM-YSZ/LSM cathode using powders with lower particle sizes clearly results in an increase in the f_{max} of the cathode charge transfer process (from ~100 Hz to ~1000 Hz), whilst exchanging the component for a CGO/LSCF-CGO/LSCF cathode almost completely removes the cathode contribution. Figure 7 illustrates the effect of exchanging the Rh/CG20 co-impregnated $LSCT_{A-}$ anode for a commonly used Ni-YSZ cermet anode and a single-phase perovskite LSCM anode (which exhibits some catalytic activity without the requirement for impregnated electrocatalysts (10)). The frequency maximum of the high-frequency arc clearly shifts when changing the composition, microstructure and type of anode material, affirming the assumption that this process does indeed pertain to anode charge transfer. It is also possible to see that the gas conversion arc changes depending on the micro/nanostructure of the anode material and that additional anode related processes appear in the spectra (e.g. at ~30 Hz for the LSCM anode), allowing full assignment of the rate limiting process using simple experiments. Finally, the Bode format plots presented in Figure 8 indicate that no change in the frequency domains of the rate limiting processes occurs when swapping the standard 6ScSZ electrolyte for a commonly employed 8YSZ electrolyte (the magnitude of the anode charge transfer arc varies due to differences in the weight loading of the Rh catalyst in the Rh/CG20 co-impregnated $LSCT_{A-}$ anodes). Aside from a change in the ohmic resistance (R_s), based upon the ionic conductivity of the electrolyte material, the electrolyte composition is not expected to affect the polarisation processes as grain boundary and/or bulk impedances in the dense electrolyte are typically observed at higher frequencies than examined during SOFC testing and have capacitances of 10^{-11} – 10^{-9} and 10^{-12} F, respectively (11).

TABLE I. A summary of the components of SOFC manufactured for component variation testing.

SOFC ID	Anode	Cathode	Electrolyte
LSM-YSZ/LSM Standard	$LSCT_{A-}$ + 13 wt. % CG20 + 2.0 wt. % Rh	LSM-YSZ/LSM Standard	6ScSZ
LSM-YSZ/LSM Fine	$LSCT_{A-}$ + 13 wt. % CG20 + 1.6 wt. % Rh	LSM-YSZ/LSM Fine	6ScSZ
CGO/LSCF-CGO/LSCF	$LSCT_{A-}$ + 11 wt. % CG20 + 2.1 wt. % Rh	CGO/LSCF-CGO/LSCF	6ScSZ
LSCM	LSCM	LSM-YSZ/LSM Standard	6ScSZ
Ni-YSZ	Ni-YSZ	LSM-YSZ/LSM Standard	6ScSZ
8YSZ	$LSCT_{A-}$ + 12 wt. % CG20 + 2.4 wt. % Rh	LSM-YSZ/LSM Standard	8YSZ

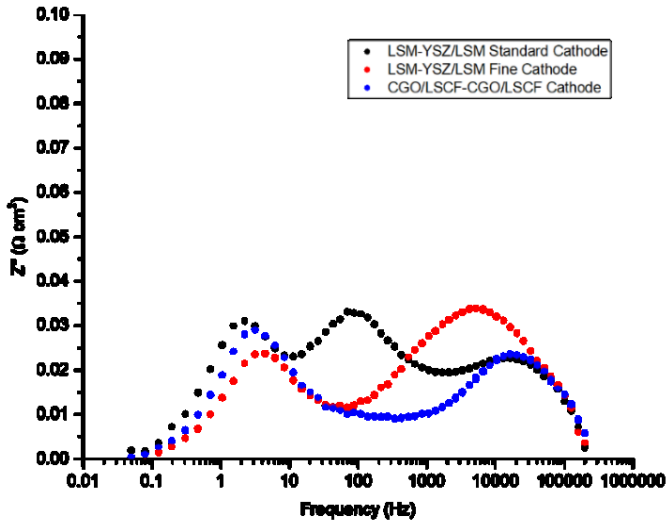

Figure 6. Comparative Bode format AC impedance spectra showing how the magnitude and frequency domain of cathode-related process changes as a function of cathode composition and microstructure (collected at 850 °C and 300 mA cm^{-2} using the HEXIS test setups).

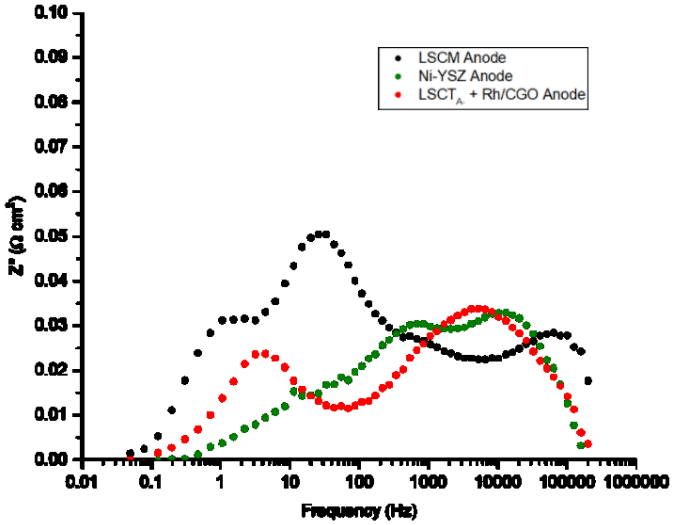

Figure 7. Comparative Bode format AC impedance spectra showing how the magnitude and frequency domain of anode-related process changes as a function of anode composition and microstructure (collected at 850 °C and 300 mA cm^{-2} using the HEXIS test setups).

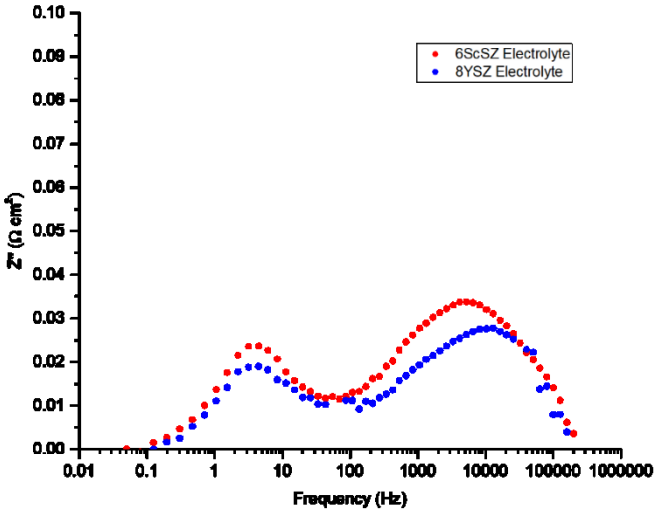

Figure 8. Comparative Bode format AC impedance spectra showing the effect of the electrolyte material on rate limiting process of the SOFC with nominally identical anodes and cathodes (collected at 850 °C and 300 mA cm^{-2} using the HEXIS test setups).

Durability Testing and Upscaling of Rh/CG20 Co-Impregnated $LSCT_{A-}$ Anodes

Durability testing of SOFC containing Rh/CG20 co-impregnated $LSCT_{A-}$ anodes was also carried out in button cell test setups at HEXIS in order to assess suitability for the upscaling process and identify typical degradation phenomena associated with these anodes, which is shown to be the component responsible for the largest polarisation resistance contribution at 850 °C, in previous sections. Figure 9 shows the change in operating voltage of a SOFC operating at 850 °C and 300 mA cm^{-2} over the first 160 hours of durability testing. The stability of the operating voltage at an industrially relevant current density is excellent during this time period and can give rise to degradation rates that rival those of state-of-the-art, commercial anodes under the same operating conditions. Further details of the long-term performance of the aforementioned SOFC will be presented in future manuscripts.

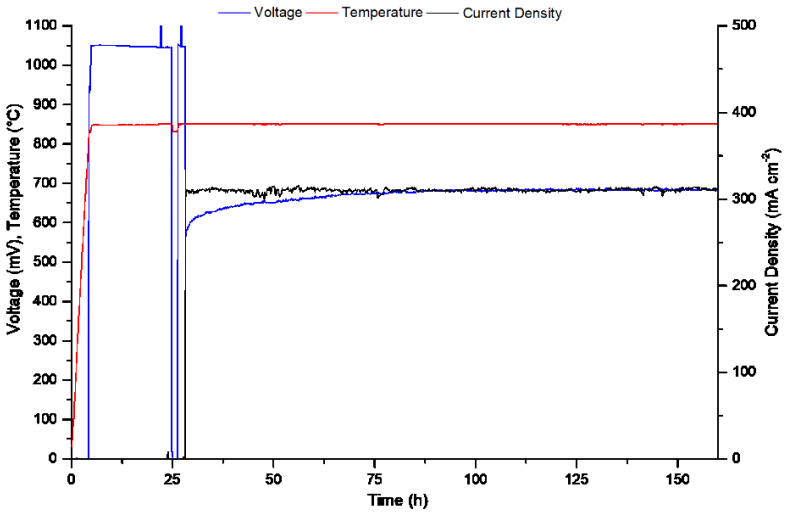

Figure 9. Galvanostatic operation profile of a SOFC containing a Rh/CG20 co-impregnated $LSCT_{A-}$ anode, for the first 160 hours of operation at 850 °C and 300 mA cm^{-2} using the HEXIS test setups.

Conclusion

This manuscript has provided an overview of research relating to the development of co-impregnated $La_{0.20}Sr_{0.25}Ca_{0.45}TiO_3$ ($LSCT_{A-}$) anodes at the University of St Andrews and HEXIS over the past ~10 years. It has been shown that ceramic processing of the limited conductivity perovskite $LSCT_{A-}$ is crucial to obtaining an optimal anode microstructure, in terms of lateral electronic conductivity and porosity for catalyst co-impregnation and gas diffusion. Furthermore, investigations into the most promising catalyst systems revealed that Rh and $Ce_{0.80}Gd_{0.20}O_{1.90}$ (CG20) co-impregnated $LSCT_{A-}$ anodes exhibit excellent performance during short-term SOFC testing. Detailed AC impedance analysis suggests that the anode charge transfer process is not discernable for this anode catalyst system above 875 °C. However, at 850 °C and below, larger polarisation resistance contributions from both the anode and cathode are rate limiting. Furthermore, the assignment of arcs in the AC impedance spectra to anode, cathode and gas conversion processes was confirmed by performing systematic variations in temperature, current density and SOFC components and measuring the AC impedance response of the SOFC. Finally, an introduction to the durability testing of these SOFC has been provided, indicating high stability of the operating voltage, at 850 °C and 300 mA cm^{-2}, over the first 160 hours of testing.

Acknowledgements

The authors would like to thank Dr Mark Cassidy and Dr Cristian D. Savaniu for providing invaluable advice on ceramic processing and conductivity measurements. In addition, the authors acknowledge funding from the University of St Andrews and HEXIS AG, as well as the EPSRC grants: EP/M014304/1 “Tailoring of Microstructural Evolution in Impregnated SOFC Electrodes” and EP/L017008/1 “Capital for Great Technologies”.

References

1. C. Sun and U. Stimming, *J. Power Sources,* **171**, 247 (2007).
2. R. Price, M. Cassidy, J. A. Schuler, A. Mai and J. T. S. Irvine, *ECS Trans*. **78**(1), 1385 (2017).
3. A. D. A. Aljaberi, *Thesis*, University of St Andrews (2013).
4. R. Price, M. Cassidy, J. G. Grolig, A. Mai and J. T. S Irvine, *J. Electrochem. Soc*. **166**, F343 (2019).
5. M. C. Verbraeken, B. Iwanschitz, A Mai and J. T. S Irvine, *J. Electrochem. Soc*. **159**, F757 (2012).
6. M. C. Verbraeken, B. Iwanschitz, E. Stefan, M. Cassidy, U. Weissen, A. Mai and J. T. S. Irvine, *Fuel Cells*, **5**, 682 (2015).
7. R. Price, M. Cassidy, J. A. Schuler, A Mai and J. T. S. Irvine, *ECS Trans*. **68**(1), 1499 (2015).
8. M. J. Jørgensen and M. B. Mogensen, *J. Electrochem. Soc*. **148**, A433 (2001).
9. S. Primdahl and M. B. Mogensen, in *Proceedings of the Fifth International Symposium on Solid Oxide Fuel Cells (SOFC-V)*, U. Stimming, S. C. Singhal, H. Tagawa and W. Lehnert, Editors, PV 97-40, p. 530, The Electrochemical Society Proceedings Series, Pennington, NJ (1997).
10. S. Tao and J. T. S Irvine, *Nat. Mater*. **2**, 320 (2003).
11. J. T. S. Irvine, D. C. Sinclair and A. R. West, *Adv. Mater.* **2**, 132 (1990).